Engineering Structures 119 (2016) 252–263

Contents lists available at ScienceDirect

Engineering Structures

journal homepage: www.elsevier.com/locate/engstruct

Aeroelastic stability of two long-span arch structures: A collaborative experience in two wind tunnel facilities

Claudio Mannini [a,*], Marco Belloli [b], Antonino M. Marra [a], Ilmas Bayati [b], Stefano Giappino [b], Fabio Robustelli [b], Gianni Bartoli [a]

[a] CRIACIV/Department of Civil and Environmental Engineering, University of Florence, Via S. Marta 3, 50139 Florence, Italy
[b] Politecnico di Milano, Department of Mechanical Engineering, Via La Masa 1, 20156 Milan, Italy

ARTICLE INFO

Article history:
Received 19 November 2015
Revised 4 April 2016
Accepted 6 April 2016

Keywords:
Arch structures
Rectangular section
Bluff body aerodynamics
Galloping
Vortex-induced vibration
Wind tunnel tests
Tuned mass damper

ABSTRACT

In this paper, a rare example of comparison between sectional and full-aeroelastic model tests is presented. Interestingly, the experiments were conducted in two very different wind tunnel facilities by different research teams. The study concerns two long-span steel arch structures recently built in Milan, Italy, for Expo 2015 World Fair. The structures have only aesthetic purposes and are therefore very flexible and light, which makes them sensitive to wind-induced excitation and prone to aeroelastic instabilities. In particular, in smooth flow an interesting phenomenon of interference between vortex-induced vibration and galloping was observed up to high values of the Scruton number. This aeroelastic instability is very dangerous as large-amplitude vibrations can occur in wind speed ranges where they are not expected, at least for what classical theories for vortex-induced vibration and quasi-steady galloping are concerned. Moreover, the provisions of Eurocode 1 resulted clearly unsuitable and non-conservative to address such a phenomenon. Despite the differences in the facilities and in the models, a good agreement was found between the results obtained in the two laboratories. The major discrepancies were observed in the transitional behavior for intermediate values of the Scruton number, the sectional model showing a more unstable behavior. The tests on the full-aeroelastic model also allowed considering the effect of the angle of wind exposure of the structures, both the in-plane and the out-of-plane vibrations of the arches and the dynamic response to turbulent wind. In particular, a set of tests in smooth flow was performed accounting for the presence of the other arch and of the surrounding buildings. A particular dynamic excitation of the in-plane flexural modes of the structures was observed in well defined ranges of flow speeds when one arch is in the wake of the other. Finally, both experimental campaigns highlighted the need for the installation of tuned mass dampers on the real structures to guarantee their safety. The effectiveness of these devices against the observed galloping-type instability was also verified through wind tunnel tests on the full-aeroelastic model.

1. Introduction

Two large arches were recently built in Milan, Italy, for Expo 2015 World Fair. These structures, visible in Fig. 1, have only an aesthetic function and therefore are very slender and light. Moreover, they present a rectangular cross section with a side ratio of 1.5 (short side parallel to the plane of the arch), which makes them prone to transverse galloping, vortex-induced vibration and to the interesting phenomenon of interference between the two types of dynamic excitation. These phenomena are crucial for the safety of the structures and hence are the main concern of this study.

This project gave the authors the great opportunity to compare the results obtained in two different wind tunnels using two types of models. In the CRIACIV[1] wind tunnel, a sectional model of the arches was tested in smooth flow, measuring static forces on the stationary model and dynamic excitation in the transverse degree of freedom on the model suspended by springs. By contrast, in the GVPM[2] laboratory, a full-aeroelastic model of the entire structure was tested and the measurements were carried out in smooth flow (both including and not including surrounding effects) and with the simulation of the atmospheric turbulent boundary layer. These

* Corresponding author. Tel.: +39 055 2758879; fax: +39 055 2758800.
E-mail address: claudio.mannini@unifi.it (C. Mannini).

[1] Interuniversity Research Centre on Building Aerodynamics and Wind Engineering.
[2] Politecnico di Milano Wind Tunnel.

http://dx.doi.org/10.1016/j.engstruct.2016.04.014
0141-0296/

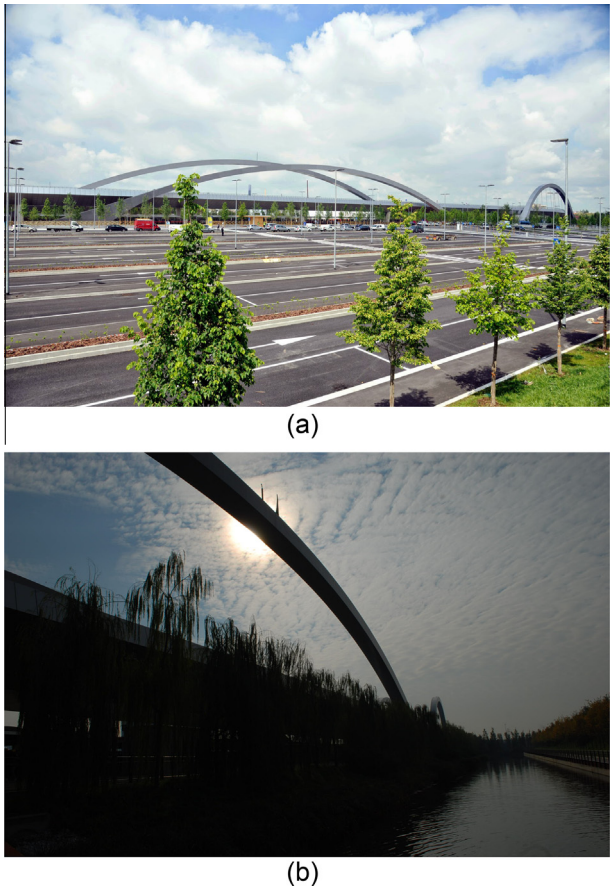

Fig. 1. View of the twin arches in the Expo 2015 area in Milan, Italy.

tests enabled considering three-dimensional features, both in-plane and out-of-plane vibrations of the arches and also various angles of exposure of the structure to the wind flow.

This is a rare occasion to compare two- and three-dimensional results from different scaled tests. Moreover, the whole measurement campaign is completed by a monitoring program that is currently running on the full-scale structure to verify the effectiveness of the damping system finally installed on the arches.

The paper starts with the description of the investigated arch structures (Section 2) and then it reports a brief overview of the aeroelastic phenomena involved in the study (Section 3). Sections 4 and 5 discuss respectively the static and dynamic experimental results obtained at CRIACIV with a sectional model and those obtained at GVPM with a full-aeroelastic model. Finally, the wind tunnel data are compared in Section 7 prior to drawing some concluding remarks.

2. Description of the structures

The structures under analysis are very long and light arches whose scope is only aesthetic. Basically, they are the main entrance gate to the Expo Milano 2015 Universal Exposition area, at the side of a highway viaduct (Fig. 1). The two arches, denoted as Arch 1 and Arch 2, are respectively 200 and 195 m long and their height is 30 and 25 m. Their planes are 32.2 m apart and their apices are misaligned by 10.8 m. The structural design is quite simple: each arch is basically a steel beam flanged to concrete foundations, the so called "noses", using stud bolts. Fig. 2 shows a picture of the structure where the concrete noses are clearly visible.

The cross section of the arches, *i.e.* their aerodynamic shape, is rectangular and it is characterized by a side ratio of 1.5. In particular, the length of the shorter side, parallel to the plane of the arch, is 2 m (D), while the other side is 3 m long (B). This shape is well known for its proneness to aerodynamic instability of galloping type [1,2].

Fig. 2. Detail of the connection between the steel arch and supporting concrete flange.

The arches have a low mass per unit length, $m = 2091$ kg/m and, being welded steel structures, they are expected to have also a low ratio-to-critical damping ζ. In fact, $\zeta = 0.3\%$ was assumed in the calculations [3]. Low mass and low damping obviously imply a low dissipation capability of the structures, and it is known that the mass-damping factor, called Scruton number, is a driving parameter in wind-induced instability problems. Herein, the resulting Scruton number was $Sc = 4\pi m\zeta/\rho D^2 = 15.8$, with $\rho = 1.25$ kg/m^3 for the air density.

The two structures have very similar natural frequencies and Table 1 summarizes the characteristics of the first vibration modes of Arch 1, whose mode shapes are shown in Fig. 3. The frequency of the first out-of-plane vibration mode is low and therefore a significant response to turbulent wind is expected. Also the frequencies of the first antisymmetric vibration modes in the plane of the arches are low, enabling vortex-induced excitation and transverse galloping instability at wind velocities lower than the design one. Finally, it is worth noting that the frequency of the first torsional mode is much higher, so that torsional wind-excitation does not represent a problem.

3. Theoretical background

As previously said, the two aesthetic arches are slender shallow structures with a rectangular cross section with a side ratio $B/D = 1.5$. When the wind is perpendicular to the plane of the arches, which seems the most harmful exposure for aeroelastic excitation (see also [4]), D and B represent respectively the cross-flow and the streamwise section dimensions. It is known that this type of structures may be prone to galloping in the vertical bending modes [1]. This is a single-degree-of-freedom dynamic instability caused by the self-excited force component in phase with the velocity. For small vibrations, this corresponds to negative aerodynamic damping that overcomes the dissipation capability of the system. During galloping, a structure exhibits nearly harmonic limit-cycle oscillations whose amplitude steadily grows by increasing the flow velocity. The practical engineering importance of this phenomenon has been shown for many types of structures, such as lighting poles and antenna masts [5]. The critical wind speed is usually obtained by the quasi-steady force criterion [6,7]. It is proportional to the Scruton number and inversely proportional to the slope in the origin of the transverse force coefficient (galloping

Table 1
Natural frequencies of the first flexural modes of Arch 1 (OP: out of plane; IP: in plane; BS: bending symmetric; BA: bending antisymmetric) calculated for the full-scale structure. The values measured for the full-aeroelastic model tested at GVPM are also reported and compared to the scaled target ones. The last column reports the model damping ratios measured in the wind tunnel.

Mode		Frequencies (Hz)			Damping (%)
#	Type	Full scale	Target	Model	Model
I	OP-BS	0.55	3.52	3.43	0.08
II	IP-BA	1.17	7.41	7.08	0.06
III	OP-BA	1.48	9.42	9.68	0.06
IV	IP-BS	1.94	12.39	12.92	0.05

instability factor) obtained through measurements on the stationary body. In this case, the critical wind speed is expected to be relatively low as the arches are light and low-damped structures (low value of the Scruton number) and the section geometry is highly unstable. The quasi-steady theory also allows the calculation of the post-critical amplitudes of vibration [8–12] and it has also been applied to the case of a yawed cylinder [13]. Nevertheless, the limits of this theory for practical applications have been highlighted in many works [14–17]. Interestingly, the galloping instability of a forward and a backward inclined square prism has recently been experimentally and numerically investigated in [17–19], which emphasize the differences as compared to the case of the same cylinder perpendicular to the incoming flow and provide a physical explanation for the results.

For slender prismatic structures with bluff cross section and sufficient afterbody (defined as the part of the cross section downstream of the separation point), also vortex-induced vibration (VIV) may be expected. This is triggered by the resonance of the force due to the alternate shedding of Kármán vortices with one mode of vibration of the structure. Nevertheless, in the case of low-damped structures, self-excited forces and nonlinear effects strongly influence the steady-state regime of oscillation, as compared to a mere linear resonance mechanism. The excitation starts at a critical wind speed which depends on the Strouhal number and disappears beyond a certain flow velocity. The amplitude of vibration and the extension of the so-called "lock-in" range depend on the mass ratio and structural damping, combined as Scruton number for conventional structures in airflow, that is for large enough mass ratios (see *e.g.* [20]). While galloping is generally expected to be a high-reduced-wind-speed phenomenon and it is therefore approached with the quasi-steady theory, VIV occurs at low reduced wind speed and definitely requires unsteady models (see *e.g.* [21] for a short review).

In smooth flow, rectangular cylinders with a side ratio in the range $0.75 \lesssim B/D \lesssim 3$ (the range is significantly different in turbulent flow) are known to be unstable with respect to galloping [1] (for lower side ratios a hard-type galloping instability is possible, that is not starting spontaneously from rest) but they are also prone to vortex-induced vibration, so that interference between the two phenomena can occur. Eurocode 1 [3] states that, if the ratio of the galloping to the VIV critical wind speed (the former calculated with the classical quasi-steady theory) is either lower than 0.7 or larger than 1.5, the two phenomena can be considered separately. Nevertheless, in the literature there are many experimental and numerical results that clearly disagree with this statement (*e.g.* [8,9,12,22–26]).

A possible interaction between VIV and galloping can be very problematic from the practical engineering point of view since it allows the onset of limit-cycle oscillations at relatively low wind speed, that is at the critical velocity for VIV, but with amplitudes unrestrictedly growing with the flow speed, as typical of galloping, even for relatively large values of the Scruton number. Moreover, large-amplitude oscillations can occur at flow speeds for which no excitation is predicted by the classical theories for VIV and galloping. Evidences of this phenomenon of interference of VIV and galloping were also found in studies on base-pivoted aeroelastic models of tall buildings with square or rectangular cross section in open-terrain turbulent flow field [27].

For very light and low-damping structures, the opposite effect has also been observed: the galloping instability, predicted at low wind speed by the quasi-steady theory, is instead suppressed by the Kármán vortex shedding (the phenomenon, wherein the auto-periodic oscillation is suppressed by the hetero-periodic oscillation, is known as "asynchronous quenching" [28,29]) and the onset of unrestricted oscillations is postponed to the VIV critical velocity. Furthermore, Eurocode 1's statement that the quasi-steady theory for galloping can be used if the corresponding critical velocity is lower than 0.7 times the vortex-resonance wind speed is definitely questionable, as in this case the assumptions standing behind this theory are heavily violated. A different approach to assess the cross-wind aeroelastic stability of structures with rectangular cross sections is provided by the ISO 4353 standard [30] and the Japanese code AIJ 1993 [31]. Therein, depending on the side ratio and the turbulence intensity (open country or urban area), the critical reduced wind speed is provided as a function of the mass-damping parameter. It was shown in [25] that these provisions give results in better agreement with experiments than Eurocode 1 for a rectangular 2:1 cylinder in a low turbulence flow.

An extensive review about the interference of VIV and galloping is reported in [2]. Therein, by collecting literature data from measurements of the galloping instability factor, a large uncertainty in its estimation was observed due to the strong dependence of its value on the test conditions (quality of model edges, Reynolds number, blockage ratio, characteristics of the oncoming flow, etc). However, the non-conservativeness of the values suggested by Eurocode 1 [3] is apparent.

4. Wind tunnel tests on the sectional model

The first set of experiments was carried out in the open-circuit CRIACIV boundary layer wind tunnel, located in Prato, Italy. The

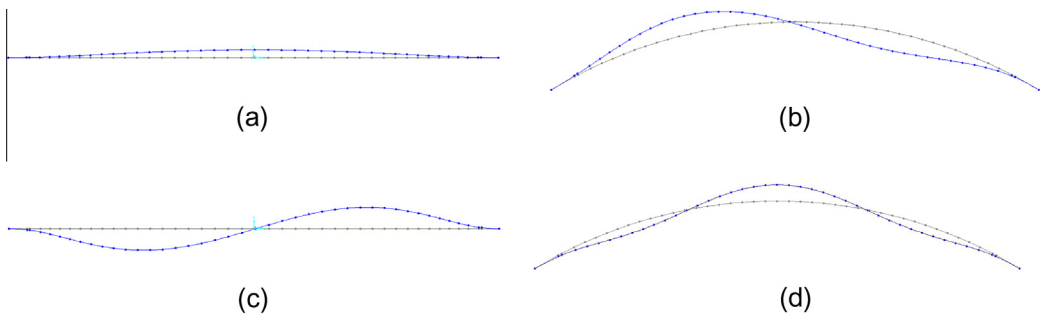

Fig. 3. Mode shapes of vibration of Arch 1: first (a), second (b), third (c) and fourth mode (d).

test section is 2.42 m wide and 1.60 m high and the wind speed can continuously be adjusted between 0 and 30 m/s.

A 1:26 scaled plywood sectional model of the arches (Figs. 4 and 5), 986 mm long (L), 116 mm wide (B) and 77 mm deep (D), was used for both static and dynamic tests. To enforce bidimensional flow conditions, rectangular plates in plywood were provided at the model ends; their dimensions (450 mm × 150 mm × 4 mm) were defined according to the principles reported in [32]. The mass of the model, end-plates and supporting carbon-fiber tube was 1.730 kg. The model was placed horizontally in the wind tunnel with the shorter side of the section perpendicular to the flow. The blockage ratio given by the model alone, calculated as D/H_{wt}, being H_{wt} the height of the wind-tunnel test section, was 4.8%. All the tests were carried out in smooth flow with a turbulence intensity below 1%.

The model was equipped with 28 pressure taps divided in four longitudinal arrays located at the center of each side of the rectangle (19 in the upper face and three on each of the other three lateral faces); registrations at a sampling frequency of 500 Hz were performed with piezoelectric pressure transducers and the system PSI DTC Initium. In all the tests, the flow speed was measured with a Prandtl tube connected to a model 239 Setra pressure transducer.

4.1. Static tests

For the static tests the model was connected to six DS EUROPE 535 QD load cells (three on each side) through a system of Cardan joints, which allowed the measurement of drag, lift and moment. The model was placed inside a rig consisting of two large plexiglass walls supported by two metallic frames connected both to the floor and the ceiling of the wind tunnel, as shown in Fig. 5. The load cells were fixed to these frames.

The aerodynamic force coefficients were determined for angles of attack ranging approximately from −10 to +10 deg with the main purpose of estimating the slope of the transverse force coefficient around the horizontal incidence, needed to predict the galloping critical velocity with the quasi-steady theory. Fig. 6 reports the drag and lift coefficients (C_D and C_L, normalized with respect to the model depth D, and positive respectively streamwise and upward) against the angle of attack α (positive nose up), evaluated for a wind speed U = 17.6 m/s, corresponding to a Reynolds number $Re = UD/\nu$ of about 90,000, being ν the air kinematic viscosity. For $\alpha = 0$ deg, the drag coefficient is 1.76, which is in good agreement with the results available in the literature [33–35].

As shown in the figure, the slope of the lift coefficient at zero angle of attack is −7.46. The corresponding galloping instability factor $a_g = -dC_L/d\alpha(0) - C_D(0)$ (see Fig. 7) results equal to 5.7. The measured value of a_g seems quite large and is very different from 1.7 provided by Eurocode 1 [3]. Nevertheless, it definitely sounds reasonable by looking at the database available in the literature for the square and rectangular 3:2 and 2:1 cylinders [2].

The power spectral densities of the lift coefficient as well as those of the pressure coefficient at the midpoint of a side of the cylinder parallel to the flow, both evaluated at various wind speeds, provide a Strouhal number $St = n_s D/U = 0.106$ (Fig. 8), which is in good agreement with most of the values reported in the literature. By contrast, the value reported in Eurocode 1 is significantly lower ($St = 0.09$) and therefore non-conservative for design purposes.

4.2. Dynamic tests

Since it is known that for structures immersed in an airflow both the lock-in amplitude of vibration and the quasi-steady galloping critical wind speed depend on the normalized mass-damping parameter and not on mass and damping separately [20], the previously mentioned value of the Scruton number Sc = 15.8 calculated for the prototype was assumed as a target to design the dynamic tests.

The rig shown in Fig. 5 was employed for the aeroelastic tests. The previously mentioned load cells were substituted by eight pre-stressed coil springs, four on each side, with an individual nominal

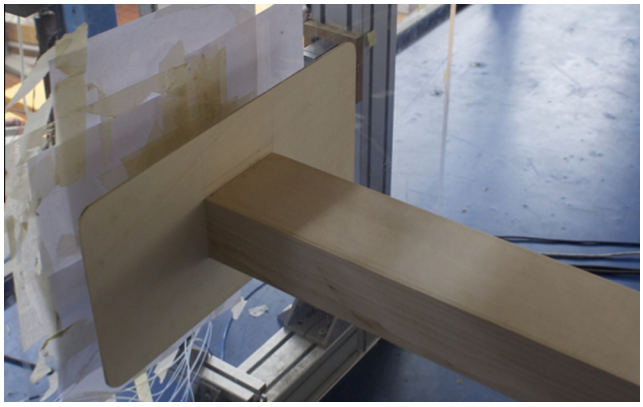

Fig. 4. Close-up view of the sectional model of the arches with end plates.

Fig. 5. View of the set-up for aeroelastic tests in the CRIACIV wind tunnel.

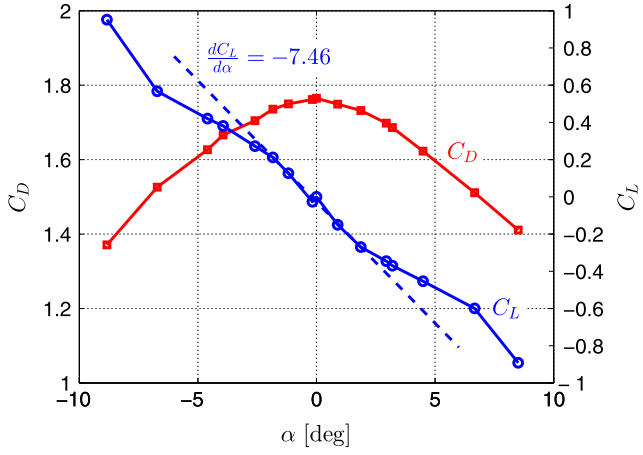

Fig. 6. Mean values of the aerodynamic drag and lift coefficients at various angles of attack (Re = 90,000).

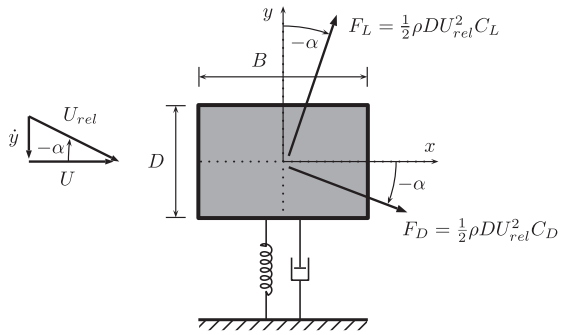

Fig. 7. Evaluation of the transverse force on a vibrating rectangular cylinder with the quasi-steady approach.

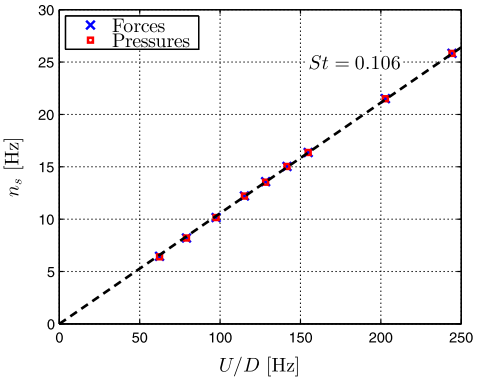

Fig. 8. Determination of the Strouhal number from the spectral peaks of lift force and local pressure time histories.

stiffness of 5340 N/m. The horizontal translation of the model was restrained by means of four long pretensioned steel cables, while the streamwise distance between the pairs of springs was large enough to guarantee a very high stiffness in the rotational degree of freedom.

The displacements of the model were recorded with three non-contact Micro-Epsilon LD 1605 laser transducers. The damping and the frequency of the system were measured through free decay tests, repeated several times. The system identification was performed with the MULS method [36]. The effective mass of the oscillating system was calculated by adding several sets of known masses and measuring the natural frequencies according to the procedure outlined in [23]. In the first basic configuration, the plunging mode had a frequency $n_0 = 14.74$ Hz, giving rise to a velocity scale 1:2.06 for the first mode of in-plane vibration of Arch 1 and 1:3.42 for the second mode. In the set-up, rolling motion was also possible, with a frequency 20% higher than the heaving one if no additional masses were provided, but it has never been significantly excited during the tests. A damping ratio $\zeta = 0.16\%$ and an effective mass of the oscillating system $M = 4.89$ kg were estimated for the heaving mode. As shown in the first row of Table 2, the Scruton number of the oscillating system in the wind tunnel in the basic configuration was 15, which is very close to the target value of 15.8. It is also apparent that the quasi-steady galloping critical wind speed $U_g = 2n_0 DSc/a_g$ in this case was significantly lower than the expected Kármán-vortex resonance wind speed $U_r = n_0 D/St$.

Assuming U_r as a reference, the Reynolds number for the model was 55,000 (see the last column of Table 2), while the corresponding full-scale value is 2,700,000. Therefore, the two Reynolds numbers differ by a factor of about 50, which is reasonable for this type of wind tunnel tests. Moreover, due to the sharp-edged cross-section geometry with small afterbody and the absence of shear-layer reattachment, no dramatic Reynolds number effects are expected, at least for small vibration amplitudes.

The dynamic tests were performed by recording the cross-flow displacements of the model at various wind speeds. The flow velocity was both increased and decreased to look for the possible presence of hysteresis loops. Fig. 9 shows that self-sustained oscillations appeared around the Kármán-vortex resonance velocity and linearly increased with the wind speed up to the maximum value of the displacement allowed by the experimental rig. Nevertheless, although it was not possible to measure the steady-state amplitude, if released from rest, the system resulted to be strongly unstable also for reduced wind speeds higher than those considered in the figure. As previously said, for the reference test configuration, the galloping critical wind speed predicted by the quasi-steady theory is significantly lower than the Kármán-vortex resonance velocity (see test case #1 in Table 2); nonetheless, the onset of galloping is prevented by vortex shedding up to U_r. Consequently, this is a clear example of the previously introduced "asynchronous quenching".

Obviously this type of response was judged unacceptable for the prototype and several other configurations were studied in order to understand which was the Scruton number necessary to suppress or opportunely reduce the oscillation amplitudes up to the design wind speed. The mass of the system was varied by adding weights at the model ends, whereas the damping was modified by wrapping the springs with electrical tape, that is rubber that dissipates energy when the model vibrates (configurations #3 to #7 in Table 2), which was found to produce practically perfect viscous damping. The tests performed, along with the main dynamic parameters for each configuration studied, are listed in Table 2; the results are summarized in Fig. 9. It can be noted that, up to Scruton numbers higher than 80, velocity-unrestricted oscillations always started around the Kármán-vortex resonance wind speed U_r instead of the predicted quasi-steady galloping critical wind speed U_g. Exactly the same amplitudes were observed if the wind speed was either increased or decreased. The vibrations showed evident amplitude modulations in the first part of the instability branch.

For high Scruton numbers ($Sc = 83$ and 86 herein) a kink in the curves is apparent close to $U/U_r = 1.5$. Afterwards, a linear trend seems to be recovered but with a reduced slope. Amplitude modulations tend to disappear after the kink, leading to nearly perfectly harmonic time histories of displacement. However, after many cycles of vibration at relatively large amplitudes, the behavior of the tape wrapping the springs may become nonlinear and the effective damping may reduce as compared to the initial or final value. This may have an influence on the nonlinear features observed for large oscillation amplitudes. However, in this range of Scruton numbers (between 80 and 90) and for flow velocities close to $1.5U_r$, the system seems to be in a transition state and the results appear more uncertain. In fact, in the test with a Scruton number of 86, the same kink is observed but at a slightly higher flow speed (and therefore amplitude) as compared to the configuration with $Sc = 83$ (see Fig. 9). Additional investigations with eddy-current dampers are needed in this mass-damping range to clarify this issue. Nevertheless, from the design point of view it is clear that the amplitudes of vibration are surely still unacceptable for Scruton numbers around 85.

By contrast, for even higher values of the Scruton number ($Sc = 201$ and 238) the oscillations suddenly dropped down to very low values after a narrow region of excitation, thus following a classical VIV behavior. Nevertheless, the non-negligible amplitude of oscillation ($y_{rms}/D = 0.016$) reached for such high Scruton numbers is surprising.

Table 2
Characteristics of the sets of measurements carried out on the sectional model in the CRIACIV wind tunnel ($m^* = \rho D^2 L/2M$ is the nondimensional mass ratio and $Re_r = U_r D/\nu$ is the Reynolds number at the Kármán-vortex resonance wind speed). The value of the galloping instability factor $a_g = 5.7$ was employed to calculate the quasi-steady galloping critical wind speed U_g.

#	n_0 (Hz)	M (kg)	ζ (%)	$m^* \cdot 10^{-4}$ (–)	Sc (–)	U_r (m/s)	U_g (m/s)	U_g/U_r (–)	$Re_r \cdot 10^3$ (–)
1	14.74	4.89	0.16	6.8	15	10.7	5.9	0.55	55.0
2	9.84	10.96	0.08	3.1	17	7.1	4.4	0.62	36.7
3	14.86	4.82	0.52	6.9	47	10.8	19.0	1.76	55.4
4	9.01	13.03	0.34	2.6	83	6.5	20.2	3.08	33.6
5	9.01	13.16	0.35	2.5	86	6.5	21.0	3.21	33.6
6	9.12	12.83	0.83	2.6	201	6.6	49.6	7.49	34.0
7	9.14	12.79	0.99	2.6	238	6.6	58.7	8.84	34.1

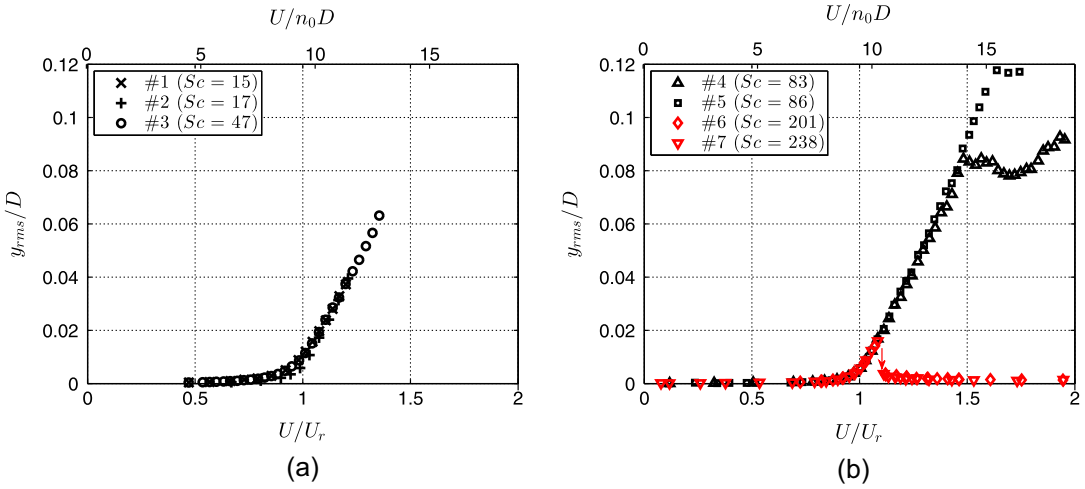

Fig. 9. Standard deviation of nondimensional model displacements for low (a) and high (b) values of the Scruton number.

In the experimental results the interference of VIV and galloping is apparent up to high values of the mass-damping parameter. According to the definition of VIV and quasi-steady galloping critical wind speed, it is possible to write:

$$\frac{U_g}{U_r} = \frac{2St}{a_g} Sc \tag{1}$$

Consequently, as shown in Table 2, a Scruton number of 86 corresponds to a ratio of critical velocities of about 3.2, whereas $Sc = 201$ corresponds to $U_g/U_r \cong 7.5$. Unfortunately, the specific set-up did not allow reaching intermediate Scruton numbers between 86 and 201, so that it was not possible to assess the value of the mass-damping factor for which VIV and galloping phenomena stop to interfere for the considered cross section. Nevertheless, one may conclude that a ratio of the critical wind speeds not lower than a threshold value falling between 3.2 and 7.5 is required to prevent the full interaction between the two aeroelastic phenomena. A similar result was also reported in [22,37], where a ratio as high as 8.4 was necessary not to observe the galloping instability onset at the Kármán-vortex resonance wind speed (although, even in this case, the critical velocity was still lower than the one predicted with the quasi-steady theory). As it has already been noted, the range of interaction between the two phenomena is very different from Eurocode 1's provisions [3], which generally exclude it outside the range $0.7 \leqslant U_g/U_r \leqslant 1.5$.

For the real arch structures, the present results mean that a value of the Scruton number around 200 is recommended and this can be achieved only by installing dampers able to provide a damping ratio as high as 3–4% for the first and second in-plane bending modes of vibration of both arches, as the corresponding vortex-resonance flow velocities are lower than the design wind speed. In addition, the structures need to be designed to withstand the amplitudes of vibration due to VIV observed also for such high values of the Scruton number (see tests #6 and #7 in Fig. 9).

5. Wind tunnel tests on the full-aeroelastic model

To confirm the results collected at CRIACIV, a wide experimental campaign was carried out at Politecnico di Milano wind tunnel (GVPM). Taking advantage of the large boundary layer test section (14 m × 4 m), a full-aeroelastic model of Arch 1 was tested along with a large model of the surrounding buildings and a rigid model of Arch 2. The models were installed on the turntable, whose diameter is equal to 13 m, so that it was also possible to investigate the influence of the exposure angle on the dynamic behavior of the structure.

The model of Arch 2 was not conceived as aeroelastic mainly to contain the high costs of the experimental campaign. Consequently, it was not possible to assess whether and to which extent the large vibrations of the upstream arch were able to excite the downstream one. By contrast, a feedback of the latter on the former seems to be excluded due to the considerable distance between the planes of the two structures (more than 16D). Nevertheless, since the oscillations of Arch 1 were confirmed to be clearly unacceptable, tuned mass dampers were judged necessary for both structures, strongly limiting the vibrations and therefore also this aeroelastic interference effect.

5.1. Full-aeroelastic model

A large scale factor (1:40) was adopted in order to have a quite high Reynolds number, comparable with those explored at CRIACIV

with the sectional model. The cross-section dimensions resulted to be in this case $D = 50$ mm and $B = 75$ mm, while the span of the arch was 5 m.

The aeroelastic model was designed to have the correct scale factor for inertia and modal deflected shape. Moreover, it was decided to scale the model dynamics according to Froude's law, having then a 1:1 scale factor on the accelerations. Then, the scale for the flow velocity was 1:6.32 and that for the frequencies resulted 6.32:1. As a consequence, the Reynolds number referred to the vortex-resonance flow speed U_r was 11,000.

The full-aeroelastic model (Fig. 10) was realized as an "equivalent model", where the required stiffness was obtained using an aluminum beam. Two different sections were used in order to reproduce the prototype variation of the stiffness at the anchorages (Fig. 2). The shape of the structure was reproduced by the external cover, which also gave the correct scaled mass per unit length (1.31 kg/m). The cover was made of machined epoxy resin CNC and was connected to the structural spine in the middle of each element, in order to avoid any elastic collaboration. Each element was very short, compared to the arch length, and there was a gap of 1 mm between two contiguous modules.

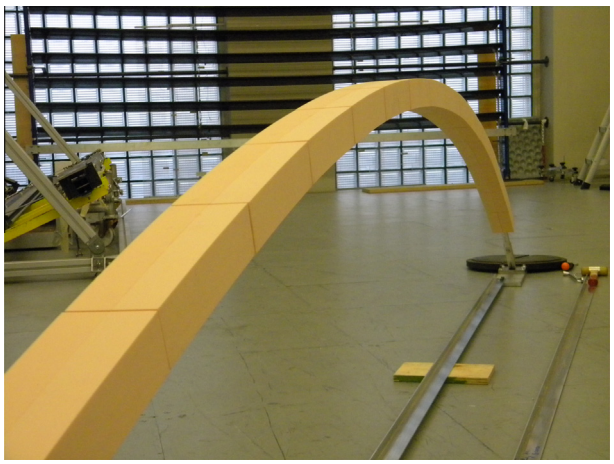

Fig. 10. Full-aeroelastic model: structural spine and cover elements.

5.2. Experimental set-up

The experimental set-up was designed to measure wind-induced accelerations, along with the shear loads and moments at the arch bases. Eight miniaturized piezoelectric accelerometers were placed on the model, four with the effective axis in the plane of the structure and perpendicular to the arch, and four perpendicular to the plane of the structure. The displacements were calculated by double integration of the accelerations. The wind-induced loads were measured using two RUAG 192 six-component force balances placed at the arch bases. The accelerometers were very light and they did not influence the natural frequencies and modal shapes of the model. Fig. 11 reports the instrument locations and their effective axis directions.

Prior to starting the tests, the model was completely characterized in terms of natural frequencies, modal shapes and damping ratios through free-decay tests. Classical modal analysis techniques were applied to define the dynamic parameters of the model, in order to assure the conformity of the scaled model to the full-scale parameters obtained using a finite-element approach. Particular care was devoted to have an as low as possible damping of the model as it is well known that the lower is the damping ratio, the more observable are all the fluid-elastic phenomena. In particular, all the junctions and connections were done by gluing and the cables of the instruments were attached to the structure.

It is apparent from Table 1 that there was a good agreement between the target and the measured values of the natural frequencies and that the damping ratios of the modes of interest were very low.

5.3. Tests in smooth flow

Smooth flow tests were carried out with the model installed alone on the turntable of the test section. The incoming wind had a flat profile with only the wind tunnel signature turbulence, that is equal to 2% with a small integral length scale of about 2 cm. Normally, this flow condition is the most severe for wind-induced instabilities, such as galloping, flutter and vortex-induced vibrations.

The arch in smooth flow was tested with six different exposures, ranging from wind perpendicular to the arch plane ($\theta = 90$ deg) up to wind parallel to its plane (either $\theta = 0$ deg or $\theta = 180$ deg), taking advantage of the symmetry of the structure. During these tests, the mean and fluctuating parts of the wind-induced loads were measured and the dynamic response was completely defined, in terms of standard deviation and maximum values of accelerations and displacements. It must be noticed that the smooth flow tests with a wind exposure of 90 deg are those most similar to the CRIACIV tests, whose results are reported in Fig. 9. The main differences are due to the three-dimensional effects.

The smooth flow tests with the very low damping level ($\zeta = 0.06\%$) of the structure in the stand-alone configuration highlight that there is a clear form of dynamic instability involving the first (antisymmetric) in-plane mode of vibration of the structure. The onset of sustained nearly harmonic oscillations occurs in a relatively gradual way around a wind speed of 20 m/s at full scale, corresponding to the vortex-resonance velocity relative to a Strouhal number very close to 0.106, as measured at CRIACIV (see Section 4.1). This is the peculiar galloping-type instability interfering with vortex-induced vibration, which was also highlighted by the sectional model tests.

Fig. 12 shows the maximum values of acceleration at the quarter span of the arch, *i.e.* close to the antinode of the first in-plane flexural mode shape; the reported results are expressed at full scale for 90-deg angle of exposure, that is wind coming perpendicular to the arch plane. Clearly, accelerations and displacements become higher than acceptable thresholds for high wind velocity and low damping ratios, that is for low Scruton numbers.

Changing the exposure angle means reducing the power input by the flow into the system, as visible in Fig. 13, where the standard deviation of the displacement at the quarter span is plotted against the exposure angle. As expected, the most severe condition is when the wind is coming perpendicular to the arch plane, that is when the three-dimensional effects are less important. For this reason, the 90-deg exposure was considered as the reference scenario to determine the damping required to avoid any form of dynamic instability.

Several tests were carried out by increasing the damping and therefore the Scruton number (Table 3). First, electrical tape was placed over the gap between the external shells and then, to have a more effective system, eddy-current dampers connected to the structural spine of the model were used. Finally, as discussed in the following section, a very high damping ratio was obtained using scaled tuned mass dampers (TMD), as these devices were also installed in the real full-scale structure (see Section 5.4).

Fig. 12 shows that, by increasing the Scruton number from 3 to 20 and then to 75, the slope of the amplitude–velocity curve slightly reduces but large values of the acceleration are quickly attained in all these cases. For a Scruton number of 80, the same pattern as for $Sc = 75$ is obtained. By contrast, for a Scruton

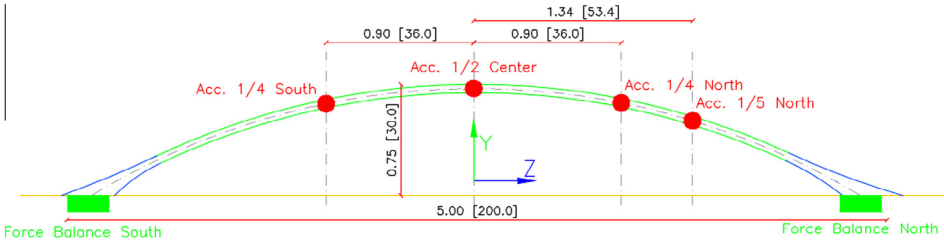

Fig. 11. Position of the instruments in the full-aeroelastic model. The dimensions are in meters at both model scale and full scale (the latter in square brackets).

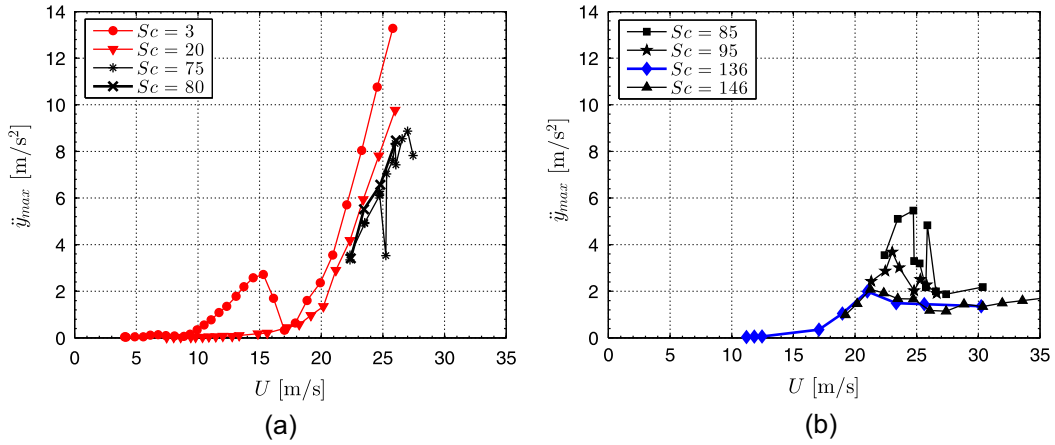

Fig. 12. Maximum value of the in-plane acceleration at a quarter of the arch span for a wind perpendicular to the arch plane: low (a) and high (b) values of the Scruton number. Flow speed and acceleration are at full scale.

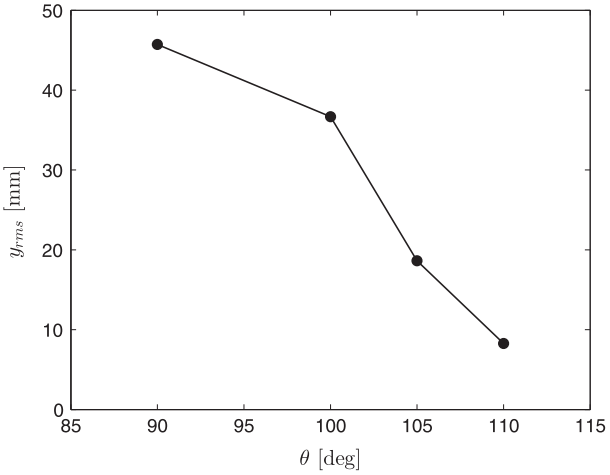

Fig. 13. Full-scale standard deviation of the in-plane displacement at a quarter of the arch span as function of the incidence angle in the horizontal plane θ, for an incoming wind speed of 22.9 m/s and a Scruton number equal to 20. $\theta = 90$ deg denotes a wind flow perpendicular to the arch plane.

number of 85, large amplitudes of oscillation are reached for full-scale wind speeds between about 20 and 26 m/s and then they drop to significantly lower values. A similar behavior is also observed for $Sc = 95$ but with a lower peak value of the acceleration. Finally, for Scruton numbers equal to 136 and 146, only a small bump in the amplitude–velocity curve is visible for flow velocities slightly higher than 20 m/s, without any significant dynamic excitation.

It is also worth noting that for very low Scruton numbers ($Sc = 3$) a self-limited excitation similar to that discussed in [2] is observed for full-scale wind speeds between about 10 and 16 m/s, that is starting around half the vortex-resonance flow velocity. This secondary excitation already disappears for a Scruton number of 20, and indeed it was not detected by the sectional model tests at CRIACIV, where values of the mass-damping factor lower than 15 were not explored.

Table 3
Scruton numbers and damping ratios of the full-aeroelastic model configurations tested.

Sc (–)	ζ (%)	Additional damping source
3	0.06	–
20	0.4	tape
75	1.5	eddy-current dampers
80	1.6	eddy-current dampers
85	1.7	eddy-current dampers
95	1.9	eddy-current dampers
136	2.7	TMDs
146	2.9	eddy-current dampers

5.4. Tuned-mass-damper design

The smooth flow tests highlighted the necessity of an adequate damping system to suppress the occurrence of galloping instability at low wind speed, so that tuned mass dampers were designed to be installed in both the full-scale structures. Therefore, also wind tunnel tests on the full-aeroelastic model with a properly scaled TMD system were carried out (Fig. 14).

More specifically, the two scaled TMDs, with masses of 22 g and 24 g, corresponding respectively to full-scale masses of 1408 kg and 1530 kg, were placed at the antinodes of the first in-plane mode shape of the structure. The damping of the secondary system was set approximately to 8%, by means of eddy-current techniques, whereas its frequency was tuned by properly choosing the section of its steel beam, as visible in Fig. 15. The TMD system allowed

reaching a damping level of about 2.7% and therefore a Scruton number of 136, as reported in Table 3. As observed in the previous section, this system allowed a complete suppression of the low-speed aeroelastic excitation involving the first in-plane flexural mode of the arch structures.

5.5. Tests in smooth and turbulent flow with surrounding

In order to investigate as thoroughly as possible different flow conditions characterizing the full-scale structure, both wind tunnel tests in a scaled atmospheric boundary layer and in a smooth incoming flow but including the obstacles surrounding the structure (Fig. 16) were carried out for a Scruton number equal to 20.

The latter confirmed the necessity to prevent large-amplitude vibrations installing TMD dampers on the real structures also with respect to the second in-plane vibration modes. In fact, Fig. 17(b) clearly shows that, whenever the arch is downstream of the small mountain visible in Fig. 16 (270 deg), the accelerations are quite small. By contrast, whenever the arch is downstream of the other arch (90 deg), a dynamic excitation due to the wake of the former occurs, increasing non-negligibly the accelerations in the range 20–30 m/s. As it is clear from Fig. 17(b), the response mainly involves the second (symmetric) in-plane mode of vibration of the structure. Nevertheless, Fig. 17(a) shows that this phenomenon can also occur with a reduced magnitude for lower velocities (about 13–15 m/s) whenever the first (antisymmetric) in-plane mode of the arch is excited. It is worth noting that the aeroelastic interaction is such that the excitations in the two modes occur for a reduced velocity of about 6.5, corresponding to a virtual Strouhal number of about 0.15.

The turbulent wind investing the reproduced area of the city and the arches was generated through spires placed at the wind tunnel inlet and roughness elements located with a suitable arrangement upstream of the model. The simulated wind profile had a full-scale roughness length equal to $z_0 = 0.1$ m and a longitudinal turbulence intensity of about 18% at heights relevant for the two arches. In Fig. 18 the standard deviation value of the acceleration at the arch quarter span is reported for turbulent flow condition with surrounding, as function of the angle of exposure. It is apparent that the accelerations are significantly smaller than for the smooth flow condition but definitely non-negligible. The main contribution to the resonant response is due to the first in-plane mode of vibration, showing a clearly random excitation. The maximum accelerations are registered when the wind blows nearly perpendicular to the plane of the structure and in particular when the instrumented arch is downstream of the previously mentioned mountain and upstream of the other arch (Fig. 16), *i.e.* for $\theta = 270$ deg.

In turbulent flow, a significant excitation of the arch out-of-plane modes was also observed with standard-deviation and maximum values of the displacement respectively of about 30 and 110 mm for a wind speed of 35 m/s, following a pattern with the exposure similar to that reported in Fig. 18. For the sake of completeness, in Fig. 19 a comparison between different test conditions is reported. More specifically, out-of-plane and in-plane full-scale displacements are shown for turbulent flow with surrounding and smooth flow, for an exposure angle of 90 deg. It is evident how the in-plane response in smooth flow is the most critical.

6. Comparison between sectional and full-aeroelastic model tests

Fig. 20 compares the results obtained at CRIACIV on the sectional model and at GVPM on the full-aeroelastic model of one of the arches with a smooth flow perpendicular to the plane of the

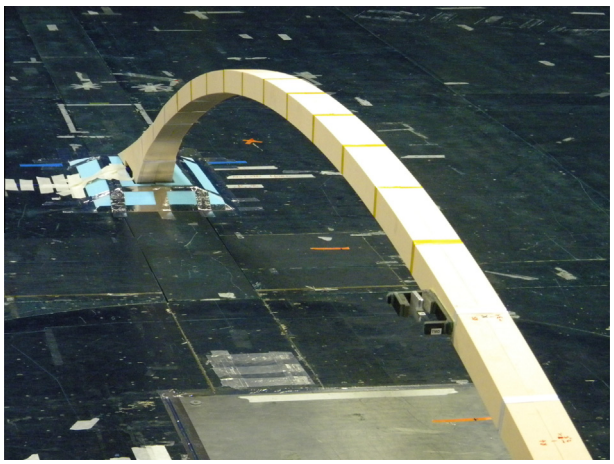

Fig. 14. Tuned mass dampers installed on the full-aeroelastic model.

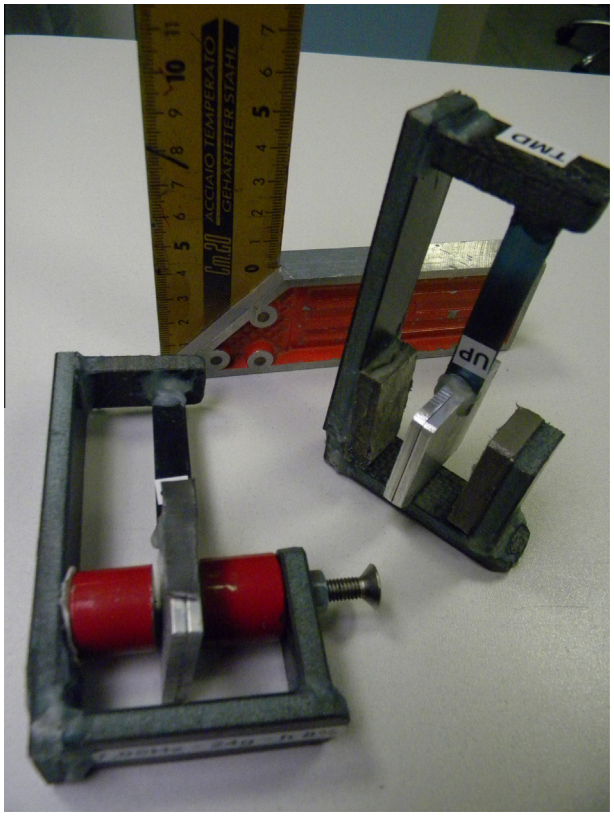

Fig. 15. Details of the tuned mass dampers.

structure for various Scruton numbers. The following main issues can be highlighted.

- For low values of the Scruton number (Fig. 20(a)), a galloping-type instability starting around the vortex-resonance flow speed is observed in both cases. Very good agreement is found on the onset velocity, that is on the Strouhal number.
- The slope of the galloping curves for the full-aeroelastic model tends to decrease as the Scruton number increases, while the amplitude–velocity pattern remains always the same for the sectional model. Nevertheless, for Scruton numbers of about 75–80, the full-aeroelastic model response amplitudes are practically the same as those measured at CRIACIV.

Fig. 16. Full-aeroelastic model in the Politecnico di Milano test section along with turbulators and surrounding.

- As shown in Fig. 20(b), the full interference of vortex-induced vibration and galloping disappears at a lower Scruton number ($Sc = 85$) for the three-dimensional model or, at least, sustained vibrations die out for lower wind speeds as compared to the sectional model tests.
- Compatible responses are registered for very high Scruton numbers.

Generally speaking, the agreement between the two sets of data is definitely satisfactory, in spite of the significant differences between the two models and set-ups, confirming the necessity of installing tuned mass dampers on the real structures to attain a damping ratio of about 3% for the first two in-plane bending modes.

As previously noticed, the main discrepancy between the two sets of results concerns intermediate Scruton numbers, close to the value for which a classical behavior with separate ranges of VIV and galloping excitation is retrieved. In this zone, the response of the arches is expected to be very sensitive to any flow, structural and geometrical difference. From this perspective, the three-dimensional characteristics of the full-aeroelastic model, a factor of about 5 in the reference Reynolds number for the two sets of tests and the slightly different free-stream turbulence in the two facilities easily justify a mismatch in the transitional behavior.

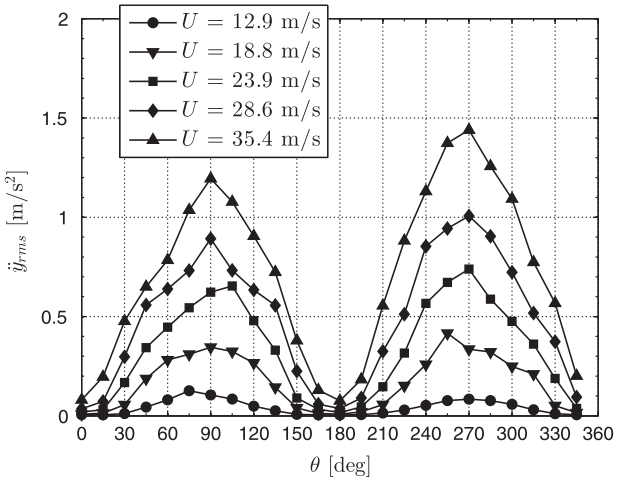

Fig. 18. Full-scale standard deviation of the in-plane acceleration at a quarter of the arch span in turbulent flow as function of incidence angle for different incoming wind velocities and exposures ($Sc = 20$).

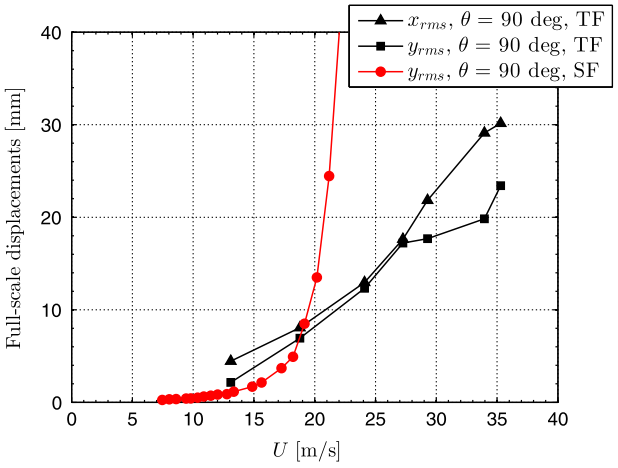

Fig. 19. Turbulent flow (TF) full-scale displacements compared with smooth flow (SF) ones at a quarter of the arch span for the wind exposure 90 deg. x_{rms} and y_{rms} denote respectively the standard deviation of the out-of-plane and in-plane displacements.

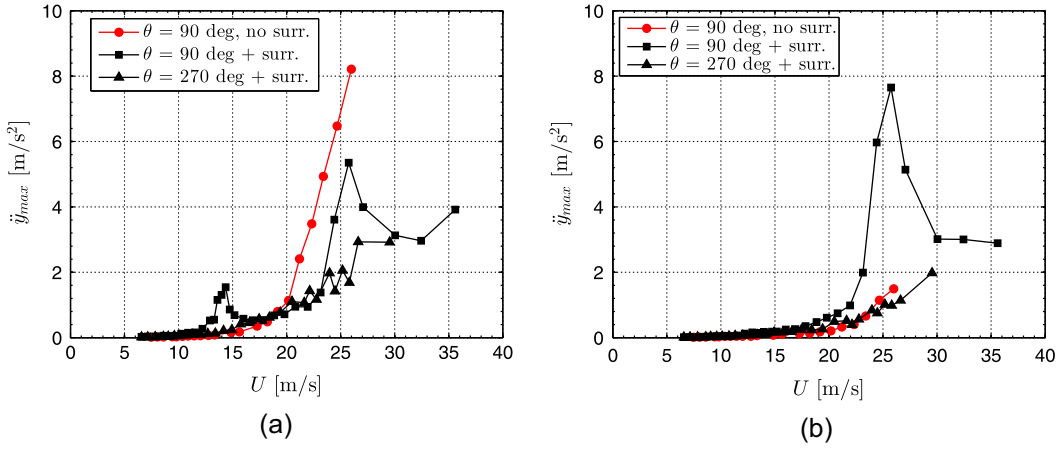

Fig. 17. Full-scale maximum values of the in-plane acceleration at one fifth (a) and a half (b) of the arch span in smooth flow, with and without surrounding ($Sc = 20$). "surr." stands for "surrounding".

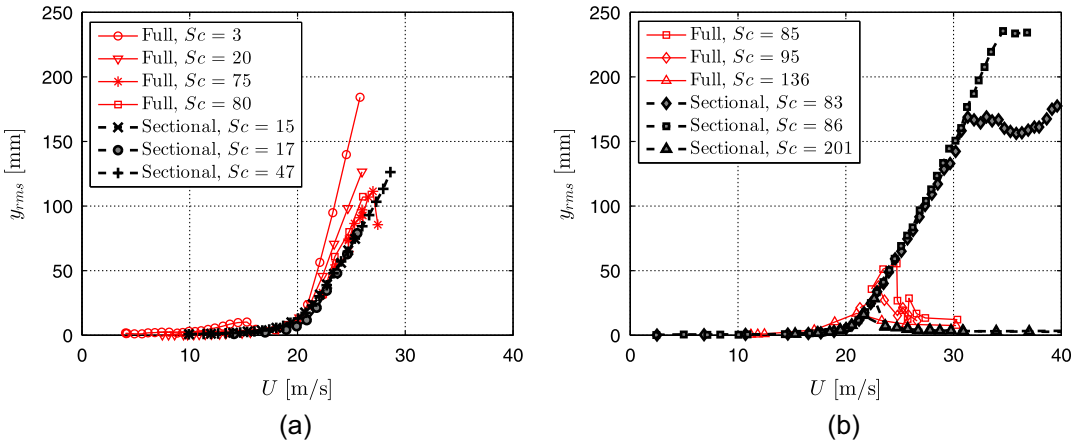

Fig. 20. Comparison between sectional (CRIACIV) and full-aeroelastic model tests (GVPM): full-scale standard deviation of the in-plane displacements as function of full-scale wind speed for low (a) and high (b) values of the Scruton number.

7. Concluding remarks

The aeroelastic behavior of two flexible and light steel arch structures was deeply investigated through two wind tunnel test campaigns in two different facilities. In the CRIACIV laboratory, static and dynamic tests were performed in smooth flow on a sectional model, whereas, in the GVPM wind tunnel, tests were carried out in smooth and turbulent flow on a three-dimensional full-aeroelastic model of one of the two arches, carefully reproducing also the surrounding area of the city.

In both experiences, a galloping-type instability starting at wind speeds close to the vortex-resonance velocity was observed in smooth flow, due to the interference of the mechanisms of vortex-induced vibration and "quasi-steady" galloping. The phenomenon is very dangerous, as it can lead to large-amplitude and velocity-unrestricted vibrations with nearly harmonic features in ranges of wind speeds where no excitation is predicted by the classical theories for vortex-induced vibration and galloping. Clearly, the prescriptions of Eurocode 1 resulted to be unsuitable and non-conservative to address such a phenomenon.

The second set of experiments in the GVPM wind tunnel was performed to understand if the results of sectional model tests were confirmed also taking into account three-dimensional features. Moreover, it was possible to consider the effect of varying the angle of wind exposure of the structure and the response to turbulent incoming flow. A significant dynamic excitation of the arches was registered only for winds blowing from directions not very different from that perpendicular to the plane of the structures.

In addition, a set of tests was performed in smooth flow accounting for the presence of the other arch and of the surrounding buildings. A particular excitation of the in-plane flexural modes was observed in well defined ranges of flow speeds, when one arch is in the wake of the other.

Despite the differences in the facilities and in the models, a good agreement is found between the results obtained in the two laboratories. The major discrepancies concern the transitional behavior for intermediate values of the Scruton number, the sectional model showing a more unstable behavior. Nevertheless, both experimental campaigns stressed the need for an increase of damping in the first two in-plane bending modes of the structures, up to values close to 3%. Consequently, tuned mass dampers were designed and installed on the real structures. The effectiveness of these devices against the observed galloping-type instability was also verified through wind tunnel tests on the full-aeroelastic model.

Acknowledgements

The authors wish to thank Politecnica Ingegneria e Architettura and Ponte Expo that allowed the publication of the wind tunnel results.

Appendix A. Supplementary material

Supplementary data associated with this article can be found, in the online version, at http://dx.doi.org/10.1016/j.engstruct.2016.04.014.

References

[1] Parkinson GV. Aeroelastic galloping in one degree of freedom. In: Wind effects on buildings and structures: proceedings of the conference held at the National Physical Laboratory, Teddington, UK, June 26–28, 1963. London: HMSO; 1965. p. 581–609.
[2] Mannini C, Marra AM, Bartoli G. VIV-galloping instability of rectangular cylinders: review and new experiments. J Wind Eng Ind Aerodyn 2014;132:109–24.
[3] EN 1991-1-4. Eurocode 1 – actions on structures – Part 1–4: general actions – wind actions; 2010.
[4] Kawai H. Effects of angle of attack on vortex induced vibration and galloping of tall buildings in smooth and turbulent boundary layer flows. J Wind Eng Ind Aerodyn 1995;54–55:125–32.
[5] Nguyen CH, Freda A, Solari G, Tubino F. Aeroelastic instability and wind-excited response of complex lighting poles and antenna masts. Eng Struct 2015;85:264–76.
[6] Glauert H. The rotation of an airfoil about a fixed axis. Reports and Memoranda 595. Aeronautical Research Committee, UK; 1919.
[7] Den Hartog JP. Transmission line vibration due to sleet. Trans Am Inst Electr Eng 1932;51(4):1074–6.
[8] Parkinson GV, Brooks NPH. On the aeroelastic instability of bluff cylinders. J Appl Mech 1961;28(2):252–8.
[9] Parkinson GV, Smith JD. The square prism as an aeroelastic non-linear oscillator. Q J Mech Appl Math 1964;17(2):225–39.
[10] Novak M. Aeroelastic galloping of prismatic bodies. J Eng Mech Div 1969;95(1):115–42.
[11] Novak M, Davenport AG. Aeroelastic instability of prisms in turbulent flow. J Eng Mech Div 1970;96(1):17–39.
[12] Novak M. Galloping oscillations of prismatic structures. J Eng Mech Div 1972;98(1):27–46.
[13] Piccardo G, Carassale L, Freda A. Critical conditions of galloping for inclined square cylinders. J Wind Eng Ind Aerodyn 2011;99(6–7):748–56.
[14] Nakamura Y, Mizota T. Unsteady lifts and wakes of oscillating rectangular prisms. J Eng Mech Div 1975;101(6):855–71.
[15] Hémon P, Santi F. On the aeroelastic behaviour of rectangular cylinders in cross-flow. J Fluids Struct 2002;16(7):855–89.
[16] Freda A, Carassale L, Piccardo G. Aeroelastic crosswind response of sharp-edge square sections: experiments versus theory. In: Proceedings of the 14th international conference on wind engineering, June 21–26, Porto Alegre, Brazil.
[17] Hu G, Tse KT, Kwok KCS. Galloping of forward and backward inclined slender square cylinders. J Wind Eng Ind Aerodyn 2015;142:232–45.

[18] Hu G, Tse KT, Kwok KCS, Zhang Y. Large eddy simulation of flow around an inclined finite square cylinder. J Wind Eng Ind Aerodyn 2015;146:172–84.
[19] Hu G, Tse KT, Kwok KCS. Aerodynamic mechanisms of galloping of an inclined square cylinder. J Wind Eng Ind Aerodyn 2016;148:6–17.
[20] Marra AM, Mannini C, Bartoli G. Van der Pol-type equation for modeling vortex-induced oscillations of bridge decks. J Wind Eng Ind Aerodyn 2011;99 (6–7):776–85.
[21] Marra AM, Mannini C, Bartoli G. Measurements and improved model of vortex-induced vibration for an elongated rectangular cylinder. J Wind Eng Ind Aerodyn 2015;147:358–67.
[22] Parkinson GV, Wawzonek MA. Some considerations of combined effects of galloping and vortex resonance. J Wind Eng Ind Aerodyn 1981;8(1-2):135–43.
[23] Bearman PW, Gartshore IS, Maull DJ, Parkinson GV. Experiments on fluid-induced vibration of a square-section cylinder. J Fluids Struct 1987;1 (1):19–34.
[24] Itoh Y, Tamura T. The role of separated shear layers in unstable oscillations of a rectangular cylinder around a resonant velocity. J Wind Eng Ind Aerodyn 2002;90(4–5):377–94.
[25] Hansen SO. Wind loading design codes. In: Fifty years of wind engineering – prestige lectures from the sixth European and African conference on wind engineering. The University of Nottingham – The University of Birmingham; 2013. p. 35–68.
[26] Mannini C, Marra AM, Bartoli G. Experimental investigation on VIV-galloping interaction of a rectangular 3:2 cylinder. Meccanica 2015;50(3):841–53.
[27] Cheng CM, Lu PC, Tsai MS. Acrosswind aerodynamic damping of isolated square-shaped buildings. J Wind Eng Ind Aerodyn 2002;90(12–15):1743–56.
[28] Minorsky N. Introduction to non-linear mechanics: topological methods, analytical methods, non-linear resonance, relaxation oscillations. Ann Arbor, MI: J.W. Edwards; 1947.
[29] Santosham TV. Force measurements on bluff cylinders and aeroelastic galloping of a rectangular cylinder Master's thesis. Vancouver, Canada: University of British Columbia; 1966.
[30] ISO 4354. Wind actions on structures; 2009.
[31] Tamura Y, Kawai H, Uematsu Y, Marukawa H, Fujii K, Taniike Y. Wind load and wind-induced response estimations in the recommendations for loads on buildings, AIJ 1993. Eng Struct 1996;18(6):399–411.
[32] Cowdrey CF. A note on the use of end plates to prevent three-dimensional flow at the ends of bluff cylinders. Aeronautical Research Council, Current Paper No. 683, HMSO, London; 1963.
[33] Nakaguchi H, Hashimoto K, Muto S. An experimental study on aerodynamic drag of rectangular cylinders. J Jpn Soc Aeronaut Space Sci 1968;16(168):1–5.
[34] Norberg C. Flow around rectangular cylinders: pressure forces and wake frequencies. J Wind Eng Ind Aerodyn 1993;49(13):187–96.
[35] Courchesne J, Laneville A. A comparison of correction methods used in the evaluation of drag coefficient measurements for two-dimensional rectangular cylinders. J Fluids Eng 1979;101(4):506–10.
[36] Bartoli G, Contri S, Mannini C, Righi M. Towards an improvement in the identification of bridge deck flutter derivatives. J Eng Mech 2009;135 (8):771–85.
[37] Smith JD. An experimental study of the aeroelastic instability of rectangular cylinders Master's thesis. Vancouver, Canada: University of British Columbia; 1962.